

Magnetic x-ray scattering at the M_5 absorption edge of Ho

H. Ott,^{1,*} C. Schüßler-Langeheine,^{1,2} E. Schierle,¹ A. Yu. Grigoriev,^{1,†} V. Leiner,^{3,4,‡} H. Zabel,³
G. Kaindl,¹ and E. Weschke¹

¹*Institut für Experimentalphysik, Freie Universität Berlin, Arnimallee 14, D-14195 Berlin-Dahlem, Germany*

²*II. Physikalisches Institut, Universität zu Köln, Zùlpicher Str. 77, D-50937 Köln, Germany*

³*Institut für Experimentalphysik/Festkörperphysik, Ruhr-Universität Bochum, D-44780 Bochum, Germany*

⁴*Institut für Werkstofforschung, WFN, GKSS Forschungszentrum, D-21502 Geesthacht, Germany*

(Received 1 February 2006; revised manuscript received 23 May 2006; published 12 September 2006)

Magnetic x-ray scattering from thin Ho-metal films at M_5 resonance reveals atomic scattering lengths up to $200r_0$ —i.e., of the same order of magnitude as predicted theoretically by Hannon *et al.* [Phys. Rev. Lett. **61**, 1245 (1988)]. The photon-energy dependence of first- and second-order magnetic satellites allows a straightforward identification of circular and linear dichroic contributions. A direct comparison to magnetic neutron scattering demonstrates the potential of the method for studies of complex magnetic structures in ultrathin films and highly diluted materials.

DOI: 10.1103/PhysRevB.74.094412

PACS number(s): 75.70.Ak, 61.10.Eq, 61.12.-q

Magnetism in thin films, nanostructures, and other complex materials is currently a field of considerable interest, where diffraction and scattering methods can provide detailed insight into spin structures and magnetic correlations. While magnetic neutron diffraction had long been the method of choice, magnetic x-ray diffraction¹ and in particular resonant magnetic x-ray diffraction using synchrotron radiation² have emerged as a complementary technique. Tuning the photon energy to the resonance of an electronic core excitation yields an element-selective enhancement of magnetic scattering.³⁻⁷ For dipole transitions, the resonant scattering length is given by^{4,8}

$$f = (\mathbf{e}' \cdot \mathbf{e})f_0 - i(\mathbf{e}' \times \mathbf{e}) \cdot \mathbf{m}f_m^c + (\mathbf{e}' \cdot \mathbf{m})(\mathbf{e} \cdot \mathbf{m})f_m^l, \quad (1)$$

with $f_0 = a(F_{+1}^1 + F_{-1}^1)$, $f_m^c = a(F_{+1}^1 - F_{-1}^1)$, and $f_m^l = a(2F_0^1 - F_{+1}^1 - F_{-1}^1)$. F_M^1 denote the energy-dependent dipole oscillator strengths according to the selection rule $\Delta M_J = 0, \pm 1$, \mathbf{e} and \mathbf{e}' are the polarization vectors of the incident and scattered x rays, respectively, and \mathbf{m} is the unit vector in the direction of the local magnetic moment. f_m^c and f_m^l are of circular and linear dichroic nature, respectively,⁸ and give rise to resonant magnetic x-ray scattering, which is particularly strong at the $L_{2,3}$ resonances of $3d$ transition metals and the $M_{4,5}$ resonances of lanthanides and actinides—i.e., in the soft x-ray region. Most of the previous work in the soft x-ray region concerns $3d$ transition metals,⁸ while lanthanides have not been studied in detail so far.

The $M_{4,5}$ resonances, characterized by strong $3d \rightarrow 4f$ dipole transitions, were discussed theoretically quite early by Hannon *et al.*, when the authors pointed out that the magnetic contribution to f can be of the same order of magnitude as the charge contribution, reaching values up to $100r_0$ (r_0 is the classical electron radius).⁴ This agrees qualitatively with the observed enhancement of the magnetic scattering intensity by a factor of $\approx 10^7$ at the M_4 resonance of uranium.⁵ A quantitative characterization of resonant magnetic x-ray scattering at the lanthanide and actinide $M_{4,5}$ resonances, however, has been impeded by the strong photon absorption.⁹

Here, we report on a comprehensive study of magnetic

x-ray scattering at the M_5 edge of holmium. By studying ultrathin Ho metal films, $|f_m^c|$ and $|f_m^l|$ could be derived quantitatively. The results and the comparison to neutron scattering demonstrate the unique potential of resonant soft x-ray diffraction for studies of thin films and complex magnetic structures.

Ho metal is ideally suited for a study of resonant magnetic soft x-ray scattering, since it orders in a helical antiferromagnetic (AFM) structure with a temperature-dependent period, which is $\approx 28 \text{ \AA}$ at 40 K,² matching the photon wavelength at the M_5 resonance. The helical modulation is essentially harmonic, dominated by a *single* wave vector. Since the magnetic structure persists down to film thicknesses of only a few monolayers (ML),^{10,11} the experiments can be carried out on thin films, for which the probed volume is limited by the film thickness rather than by the x-ray probing depth and therefore absorption effects on the scattered intensity across resonance are minimized. For the heavy lanthanides, the assignment of the dipole transitions observed at the M_5 resonance is straightforward, and circular and linear dichroic components can be readily identified.¹²

The experiments were carried out with an ultrahigh-vacuum- (UHV-) compatible ($\Theta/2\Theta$) diffractometer, using thin Ho metal films grown *in situ* on a W(110) substrate¹¹ as well as samples prepared *ex situ* by molecular-beam epitaxy (MBE) on *a*-plane sapphire;¹⁰ the latter samples were grown on a Nb/Y buffer layer and were capped with an Y/Nb layer to avoid oxidation. X-ray diffraction data were recorded at the U49/1-SGM undulator beamline of the Berliner Elektronenspeicherring für Synchrotronstrahlung (BESSY) with the incident x rays linearly polarized in the diffraction plane (π polarization). The reflected x-ray intensities were recorded with a Si photodiode mounted behind a rectangular slit. Comparative neutron diffraction experiments were performed at the ADAM neutron reflectometer at the Institute Laue-Langevin (ILL), Grenoble, using neutrons with a wavelength of 4.41 \AA .

The resonant enhancement of magnetic x-ray scattering and the strong absorption at the Ho M_5 resonance are illustrated in Fig. 1(a). The figure shows specular reflectivity

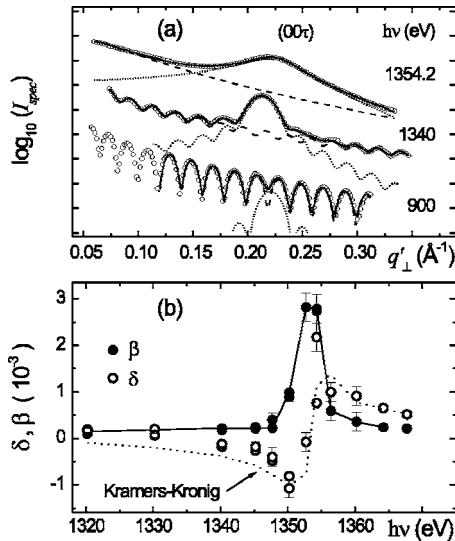


FIG. 1. (a) Specularly reflected intensities (I_{spec}) from a 110-ML Ho film grown on W(110) as a function of the perpendicular momentum transfer q'_{\perp} , recorded at the given photon energies; the data are plotted on a logarithmic scale and vertically offset to facilitate comparison. Solid lines represent fits as described in the text. The dotted and dashed curves denote the contributions from magnetic and charge scattering, respectively. (b) Optical parameters δ and β of Ho metal in the M_5 region. The solid line through the data points for β serves as a guide to the eyes.

curves of a 110-ML (monolayer) Ho film grown on W(110), recorded at 40 K—i.e., well below the bulk Néel temperature $T_N = 131.2$ K. $q'_{\perp} = (4\pi/\lambda)\sin(\Theta)$ refers to the nominal momentum transfer perpendicular to the surface, which has not been corrected for absorption and refraction. Far below the resonance at $h\nu = 900$ eV, the reflectivity is dominated by charge scattering; the intensity oscillations (Kiessig fringes) are due to interference of x rays scattered from the film surface and the Ho/W interface.¹³ Even at this energy magnetic scattering is observable, leading to the less-pronounced minimum around $q'_{\perp} = 0.22 \text{ \AA}^{-1}$. At $h\nu = 1340$ eV, closer to the M_5 resonance, the magnetic-structure peak labeled (00τ) is strongly enhanced. The magnetic origin of the peak is verified by its temperature dependence, with the peak vanishing at T_N as shown further below. At the resonance maximum ($h\nu = 1354.2$ eV), the strong photon absorption alters the reflectivity curve substantially: The magnetic peak is broadened due to the reduced number of layers that contribute to the magnetic signal,⁹ and the Kiessig fringes are suppressed, since the x rays no longer reach the Ho/W interface.

For a quantitative description of resonant magnetic scattering, the optical parameters δ and β of Ho metal were determined across the Ho M_5 resonance; $n = 1 - \delta + i\beta$ is the complex index of refraction. The simple layer structure of Ho/W(110) permits a straightforward quantitative fit analysis of the reflectivity curves. The spectra were described by a superposition of the Fresnel reflectivity of a Ho slab on a semi-infinite substrate and a magnetic diffraction peak. We fitted the Fresnel reflectivity in the framework of the dynamical theory of reflectivity as demonstrated by Parratt.¹⁴ Refraction and absorption were included using a complex scat-

tering vector $q_{\perp} = (4\pi/\lambda)\sin(\sqrt{\Theta^2 - 2\delta + 2i\beta})$. The combined interface and surface roughness was taken into account by a Debye-Waller-like damping of the reflected intensity $I_R^{Fresnel}$ with a mean structural roughness σ_s : $I_R = I_R^{Fresnel} e^{-q_{\perp}^2 \sigma_s^2}$.¹³

Far from resonance, the tabulated values of δ and β are reliable and can be used to fit the data in order to obtain the structural parameters: With $\delta = 0.97614 \times 10^{-3}$ and $\beta = 0.32688 \times 10^{-3}$ at $h\nu = 900$ eV,¹⁵ we obtain a thickness of 110 ML [(309 \pm 1) \AA] and a combined surface and interface roughness of (1.0 \pm 0.5) \AA .

Superimposed on the reflectivity, the magnetic peak is given by the structure factor¹⁶

$$S(q_{\perp}) \propto P e^{-q_{\perp}^2 \sigma_m^2 / 2} \sum_{m=1}^N e^{imd(q_{\perp} - q_{\tau})}, \quad (2)$$

where N is the number of atomic layers. q_{\perp} is the momentum transfer in specular geometry and q_{τ} the magnetic modulation wave vector. Furthermore, a mean magnetic roughness σ_m and an angle-dependent polarization factor P were included. The latter is due to the polarization-dependent prefactors of f_m^c and f_m^d in Eq. (1) and is available for a magnetic helix.⁸ The refraction and absorption corrections to the shape of the magnetic peak were again introduced by a complex scattering vector. The model works for all photon energies and down to small scattering angles until the reflectivity is altered by the footprint effect—i.e., when the projection of the x-ray spot size on the sample surface becomes larger than the sample. With the structural parameters determined, only δ , β , and the intensities of the Fresnel reflectivity and the magnetic satellite were varied as a function of photon energy.

The optical constants at a given photon energy were obtained from a fit of the respective reflectivity curve [solid line through the data points in Fig. 1(a)]. This procedure yields δ and β as plotted in Fig. 1(b) in an essentially independent way; they are consistent as verified by the Kramers-Kronig transformation of β [dotted line, Fig. 1(b)], which reproduces δ rather well. At the resonance maximum, we obtain $\beta = (2.8 \pm 0.3) \times 10^{-3}$, which is smaller than reported by Vicentin *et al.*,¹⁷ but using their relative values of Gd and Ho, it fits nicely to recent values for Gd.¹⁸

$\beta = 2.8 \times 10^{-3}$ at 1353 eV corresponds to a photon attenuation length of $\approx 260 \text{ \AA}$. Taking into account the angle of incidence at the magnetic peak position, an effective probing depth of only $\approx 28 \text{ \AA}$ is obtained. Thus, ultrathin films are required for a quantitative study of magnetic scattering in order to avoid substantial absorption corrections.¹⁹ While such films can be readily prepared on W(110), they exhibit a larger helix period as in the bulk—i.e., a smaller q_{τ} .¹¹ Therefore, while Ho/W(110) is well suited for the determination of β and δ from reflectivity curves, the MBE films are preferable for a quantitative determination of f , since q_{τ} is shifted to larger values due to the influence of the Y/Ho interfaces,¹⁰ resulting in a rather small background of charge scattering at the position of the magnetic peak.

Figure 2(a) shows the specular reflectivity of a 46- \AA (16-ML) MBE film recorded with π -polarized incident x rays slightly below the M_5 resonance maximum. The reflectivity exhibits two pronounced magnetic peaks, (00τ) at scattering

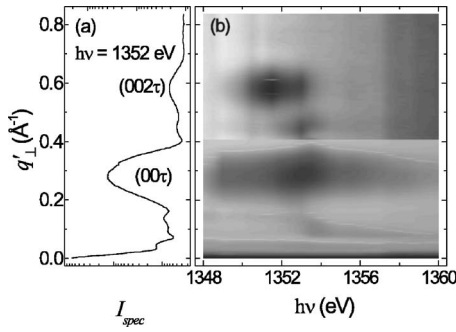


FIG. 2. (a) I_{spec} from a 16-ML Ho MBE film on a logarithmic scale, recorded close to the M_5 resonance maximum. (b) Gray-scale plot of the specularly reflected intensity as a function of the photon energy. The values for $q'_\perp > 0.4 \text{ \AA}^{-1}$ were plotted on a different gray scale to emphasize the second-order magnetic satellite.

vector $q'_\perp \approx 0.3 \text{ \AA}^{-1}$ and (002τ) at $q'_\perp \approx 0.6 \text{ \AA}^{-1}$, which are broader than in the case of the 110-ML film; still they are well pronounced above the charge scattering background. The shape of the reflectivity background here is less simple than in the case of Ho/W(110) since the layer structure is more complicated and it falls more rapidly off because of the roughness due to the intermixing of Ho and Y at the interfaces. The (00τ) peak, already seen in Fig. 1, is due to f_m^c , with a polarization factor *linear* in \mathbf{m} . The (002τ) was not observed out of resonance and is thus a pure resonance effect due to f_m^l .²⁰ With a polarization factor *quadratic* in \mathbf{m} , f_m^l gives rise to a resonant peak at (002τ) , since \mathbf{m}^2 oscillates with half the magnetic period. Generally, the linear dichroic term f_m^l probes elements that preserve time-reversal symmetry;²¹ therefore, it can be used to study the ordering of quadrupole moments in nonspherical charge densities. In the present case of AFM Ho metal, however, a distinction of quadrupolar and spin linear dichroism is of no significance, since the strong spin-orbit interaction of the atomiclike $4f$ states couples the arrangement of the quadrupole moments to the spin structure.²² Thus, the (00τ) and (002τ) can be entirely described by f_m^c and f_m^l , respectively, and both contributions are readily identified, since (00τ) and (002τ) are well separated in momentum space.

The different origins of (00τ) and (002τ) are reflected in the photon-energy dependences displayed in Fig. 2(b), with maxima at different photon energies. From the integrated intensities I_τ and $I_{2\tau}$ of the first (τ -) and second (2τ -) order satellites, the circular and linear magnetic scattering lengths, respectively, were determined:

$$\frac{d\sigma_{\tau,2\tau}}{d\Omega} = P_{\tau,2\tau}^2 |f_m^{c,l}|^2 \int_{\tau,2\tau} |S(q)|^2 d\Omega = \frac{I_{\tau,2\tau}}{I_0}. \quad (3)$$

Here I_0 is the intensity of the incident x rays measured with the same Si diode as the reflected intensities. The integration covers the momentum-space volume of the respective magnetic peak,²³ assuming that f_{circ} and f_{lin} are constant across the peak. With polarization factors P_τ and $P_{2\tau}$ for the magnetic helix⁸ and with absorption corrections using the β val-

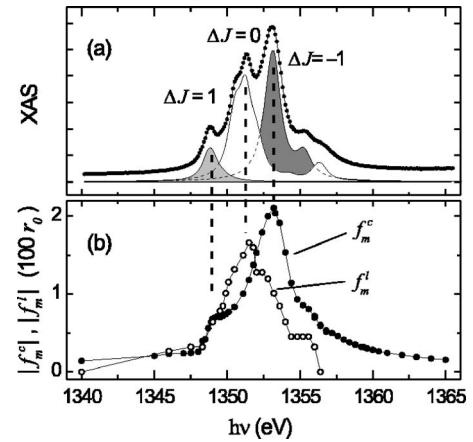


FIG. 3. (a) Absorption data recorded via sample drain current from a 31-ML Ho film on W(110) as a function of photon energy across the Ho M_5 resonance. The subspectra represent calculated $\Delta J = 0, \pm 1$ transitions from Ref. 12. (b) Scattering lengths $|f_m^c|$ and $|f_m^l|$ derived from the data of Fig. 2.

ues from the previous analysis (Fig. 1), we obtain $|f_m^c|$ and $|f_m^l|$.

The results on magnetic scattering at the Ho M_5 resonance are summarized in Fig. 3. The top panel (a) displays the sample drain current as a function of photon energy, which is proportional to the absorption coefficient.²⁴ The absorption spectrum exhibits a $3d^9 4f^{11}$ final-state multiplet, which is well understood on the basis of atomic multiplet calculations and can be separated into three distinct contributions according to the dipole selection rule $\Delta J = 0, \pm 1$ (subspectra).^{12,25} In the presence of magnetic order, the J states are split into M_J sublevels and the transitions are governed by the selection rule $\Delta M_J = 0, \pm 1$. At the M_5 resonances of the heavy lanthanides, the probabilities for a given ΔJ transition are dominated by a *single* M_J value and the selection rule $\Delta J = 0, \pm 1$ corresponds approximately to $\Delta M_J = 0, \mp 1$, respectively. Hence, the three groups in Fig. 3(a) represent essentially the respective $|F_M^1|^2$.²⁵

The resonant magnetic scattering lengths, derived from the data of Fig. 2, are plotted in Fig. 3(b) as a function of photon energy. They reveal a clear correspondence to the subspectra of Fig. 3(a), since the transitions $\Delta M_J = 0, \pm 1$ are well separated in energy.^{12,25} $|f_{circ}^c|$ peaks at the position of the $\Delta M_J = \pm 1$ maxima, while $|f_{lin}^l|$ peaks at the maximum of the $\Delta M_J = 0$ transitions, as indicated by the vertical lines in Fig. 3. This clearly identifies the circular and linear dichroic components of the scattering length [Eq. (1)]. We obtain $|f_m^c| = 200r_0$ and $|f_m^l| = 160r_0$ at their respective resonance maxima, which is somewhat larger but of the same order of magnitude as the values of $100r_0$ predicted by Hannon *et al.*⁴

The huge resonant enhancement of magnetic x-ray scattering at the M_5 resonance is further illustrated in Fig. 4, which compares resonant magnetic x-ray diffraction with magnetic neutron diffraction from the 46- \AA film. Even with the high neutron flux at the ILL, count rates in the magnetic diffraction peak are ≈ 10 neutrons/s (left panel), although exploiting essentially the whole sample area of $15 \times 20 \text{ mm}^2$. In the x-ray case, count rates from the same sample were $\approx 10^8$ photons/s, using an area of only ≈ 200

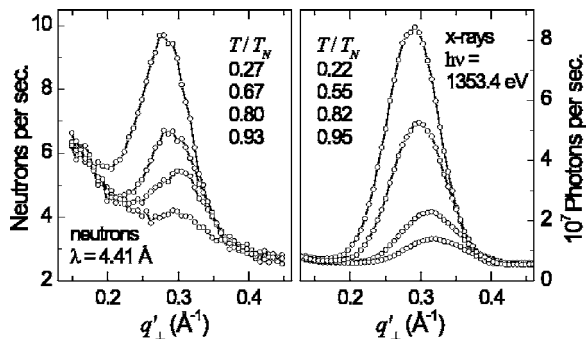


FIG. 4. Magnetic (00τ) diffraction peaks from a 16-ML MBE-grown Ho film at different temperatures (given in units of the ordering temperature T_N). Left: neutron diffraction. Right: resonant x-ray diffraction at the Ho M_5 resonance maximum. The total counting time per data point was 510 s and 1 s for the neutron and x-ray data, respectively.

$\times 500 \mu\text{m}^2$, as given by the size of the beam spot on the sample. Besides the strong resonance, this is due to the high photon flux available at undulator beamlines, making soft x-ray diffraction favorable to study thin-film magnetism.

There are more fundamental differences between neutron and resonant magnetic x-ray scattering, caused by the different ways in which these methods probe the magnetic structure. Besides the different time scales probed by neutrons and x rays, which leads to a different sensitivity to fluctuations, neutron scattering is sensitive to the magnetization density,²⁶ which is why the method directly probes the order parameter $O(T)$. Resonant magnetic x-ray scattering, on the other hand, probes—also in contrast to nonresonant magnetic x-ray scattering—the orientation of the local magnetic moment.⁸ At this point the question arises as to how the local quantity probed by the different scattering contributions in resonance is related to the magnetic order. Figure 5(a) shows the temperature dependence of the (00τ) and (002τ) satellite intensities, recorded from a 89-ML MBE Ho film and corrected for absorption. Both curves look quite different, reflecting the different ways the magnetic scattering length is related to m [Eq. (1)]. Taking the m and m^2 dependence of the respective scattering length in Eq. (1) into account the order parameter can be assumed to be $\propto I_\tau^{1/2}$ for the (00τ) and $\propto I_{2\tau}^{1/4}$ for the (002τ) satellites while experimentally a small deviation from the factor of 2 between the exponents was

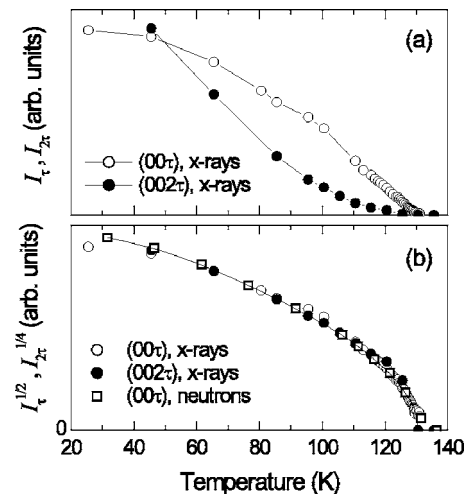


FIG. 5. (a) Comparison of the (00τ) and (002τ) satellite intensities as obtained from a 89-ML MBE Ho film by resonant x-ray diffraction. (b) Temperature dependence of the magnetic order parameter. The data were obtained from the satellite intensities in (a) and additionally from the (00τ) satellite measured by neutron diffraction from the same film.

observed.²⁷ Indeed, for both satellites a such determined O shows the same temperature dependence and is also in good agreement with $O(T)$ determined from the same sample by neutron diffraction as displayed in Fig. 5(b).²⁸

A similar magnetic sensitivity can be expected for the other lanthanides, which also exhibit strong dichroism at the $M_{4,5}$ resonance. Hence, resonant magnetic x-ray scattering using synchrotron radiation opens interesting new possibilities for the study of complex magnetic ordering phenomena in lanthanide-based materials, even if the respective magnetic ions are highly diluted. These include temperature-dependent studies in the region of short-range magnetic correlations in ultrathin films as well as the exploitation of the tunable photon absorption (Fig. 1) for magnetic depth profiling, with probing depths of ≈ 30 to 300 Å.

The expert support and excellent beamline conditions at BESSY are gratefully acknowledged. We acknowledge helpful discussions with M. W. Haverkort. Financial support came from the BMBF, Projects No. 05KS1KEE/8 and 03ZA6BC1, the DFG, Sfb-290, TPA06, and the Landesministerium NRW für Wissenschaft und Forschung.

*Present address: II. Physikalisches Institut, Universität zu Köln, Zùlpicher Str. 77, D-50937 Köln, Germany.

[†]Present address: Materials Science and Engineering Department, University of Wisconsin–Madison, 1509 University Avenue, Madison, WI 53706, USA.

[‡]Present address: EUFO 3450, European Commission, L-2920 Luxembourg.

¹F. de Bergevin and M. Brunel, Phys. Lett. **39A**, 141 (1972).

²Doon Gibbs, D. E. Moncton, K. L. D'Amico, J. Bohr, and B. H. Grier, Phys. Rev. Lett. **55**, 234 (1985).

³Doon Gibbs, D. R. Harshman, E. D. Isaacs, D. B. McWhan, D. Mills, and C. Vettier, Phys. Rev. Lett. **61**, 1241 (1988).

⁴J. P. Hannon, G. T. Trammell, M. Blume, and D. Gibbs, Phys. Rev. Lett. **61**, 1245 (1988).

⁵E. D. Isaacs, D. B. McWhan, C. Peters, G. E. Ice, D. P. Siddons, J. B. Hastings, C. Vettier, and O. Vogt, Phys. Rev. Lett. **62**, 1671 (1989).

⁶J. M. Tonnerre, L. Sève, D. Raoux, G. Soullié, B. Rodmacq, and P. Wolfers, Phys. Rev. Lett. **75**, 740 (1995).

⁷Maurizio Sacchi, Coryn F. Hague, Luca Pasquali, Alessandro

- Mirone, Jean-Michel Mariot, Peter Isberg, Eric M. Gullikson, and James H. Underwood, *Phys. Rev. Lett.* **81**, 1521 (1998).
- ⁸S. W. Lovesey and S. P. Collins, *X-ray Scattering and Absorption by Magnetic Materials*, (Clarendon Press, Oxford, 1996), p. 180ff.
- ⁹N. Bernhoeft, A. Hiess, S. Langridge, A. Stunault, D. Wermeille, C. Vettier, G. H. Lander, M. Huth, M. Jourdan, and H. Adrian, *Phys. Rev. Lett.* **81**, 3419 (1998).
- ¹⁰V. Leiner, D. Labergerie, R. Siebrecht, Ch. Sutter, and H. Zabel, *Physica B* **283**, 167 (2000).
- ¹¹C. Schüßler-Langeheine, E. Weschke, A. Yu. Grigoriev, H. Ott, R. Meier, D. V. Vyalikh, Chandan Mazumdar, C. Sutter, D. Abernathy, G. Grübel, and G. Kaindl, *J. Electron Spectrosc. Relat. Phenom.* **114-116**, 953 (2001).
- ¹²J. B. Goedkoop, B. T. Thole, G. van der Laan, G. A. Sawatzky, F. M. F. de Groot, and J. C. Fuggle, *Phys. Rev. B* **37**, 2086 (1988).
- ¹³M. Deutsch and B. Ocko, in *Encyclopedia of Applied Physics*, edited by G. L. Trigg and E. H. Immergut (Wiley-VCH, Weinheim, 1998), Vol. 23, p. 479.
- ¹⁴L. G. Parratt, *Phys. Rev.* **95**, 359 (1954).
- ¹⁵B. L. Henke, E. M. Gullikson, and J. C. Davis, *At. Data Nucl. Data Tables* **54**, 181 (1993); http://www-cxro.lbl.gov/optical_constants
- ¹⁶M. Blume and D. Gibbs, *Phys. Rev. B* **37**, 1779 (1988).
- ¹⁷Flávio C. Vicentin, Stefano Turchini, Francisco Yúbero, Jan Vogel, and Maurizio Sacchi, *J. Electron Spectrosc. Relat. Phenom.* **74**, 187 (1995).
- ¹⁸J. E. Prieto, F. Heigl, O. Krupin, G. Kaindl, and K. Starke, *Phys. Rev. B* **68**, 134453 (2003).
- ¹⁹P. D. Spencer, S. B. Wilkins, P. D. Hatton, S. D. Brown, T. P. A. Hase, J. A. Purton, and D. Fort, *J. Phys.: Condens. Matter* **17**, 1725 (2005).
- ²⁰D. Mannix, S. Coad, G. H. Lander, J. Rebizant, P. J. Brown, J. A. Paixão, S. Langridge, S. Kawamata, and Y. Yamaguchi, *Phys. Rev. B* **62**, 3801 (2000).
- ²¹S. B. Wilkins, J. A. Paixão, R. Caciuffo, P. Javorsky, F. Wastin, J. Rebizant, C. Detlefs, N. Bernhoeft, P. Santini, and G. H. Lander, *Phys. Rev. B* **70**, 214402 (2004).
- ²²M. Amara and P. Morin, *J. Phys.: Condens. Matter* **10**, 9875 (1998).
- ²³ $|f_m^c|$ and $|f_m^d|$ are calculated taking the Lorentz factor L and the number of scattering atoms n into account: $\int |S(q)|^2 d\Omega = nL$. L accounts for the experimental momentum-space integration, which depends on details like, e.g., the momentum-space volume covered by the detector area (Ref. 29). n enters via the atomic density of Ho $\rho = n/V = 3.2 \times 10^{-2} \text{ \AA}^{-3}$, where the interaction volume V is given by the size of the beam spot, the incidence angle, and the film thickness. The size of the beam spot, which is not known accurately, also enters I_0 and hence cancels in the ratio I_r/I_0 . The sample was assumed to be fully magnetized at 30 K and the Debye-Waller factor was assumed to be 1.
- ²⁴B. T. Thole, G. van der Laan, J. C. Fuggle, G. A. Sawatzky, R. C. Karnatak, and J.-M. Esteva, *Phys. Rev. B* **32**, 5107 (1985).
- ²⁵J. Ph. Schillé, J. P. Kappler, Ph. Sainctavit, C. Cartier dit Moulin, C. Brouder, and G. Krill, *Phys. Rev. B* **48**, 9491 (1993).
- ²⁶M. F. Collins, *Magnetic Critical Scattering* (Oxford University Press, Oxford, 1989).
- ²⁷G. Helgesen, J. P. Hill, T. R. Thurston, Doon Gibbs, J. Kwo, and M. Hong, *Phys. Rev. B* **50**, 2990 (1994).
- ²⁸The x-ray and neutron diffraction data were recorded using different sample environments. Despite careful temperature calibration, we had to shift the neutron data by 5 K to higher values to fit the data obtained by x-ray diffraction.
- ²⁹J. Als-Nielsen and D. McMorrow, *Elements of Modern X-Ray Physics* (Wiley, New York, 2001).